Modeling dynamics and thermodynamics of icebergs in the Barents Sea from 1987 to 2005

I. Keghouche,[1] F. Counillon,[1] and L. Bertino[1]

Received 2 February 2010; revised 2 July 2010; accepted 6 October 2010; published 24 December 2010.

[1] A modeling study of iceberg drift characteristics in the Barents and Kara seas for the period 1987–2005 is presented. Maps of iceberg density and potential locations subject to grounding complement sparse existing oceanographic and aerial field survey campaigns. The model suggests preferential pathways from the most important calving sources. Icebergs originating from Franz Josef Land have the largest spread over the domain. Simulations confirm the previously observed seasonal cycle of the southernmost extent of the icebergs. Strong interannual variability of the iceberg extent with a weak decreasing trend occurs, similar to the observed sea ice extent. Analysis of the atmospheric forcing reveals that years with anomalous northerly winds enhance the southward iceberg extension. Northerly winds also have a positive delayed impact on the iceberg extent. They limit the inflow of Atlantic Water into the Barents Sea and, therefore, its heat content the following year, increasing the mean age of icebergs and thus their potential extension. Finally, the model is able to reproduce the observed extreme iceberg extension southeast of the Barents Sea in May 2003.

Citation: Keghouche, I., F. Counillon, and L. Bertino (2010), Modeling dynamics and thermodynamics of icebergs in the Barents Sea from 1987 to 2005, *J. Geophys. Res.*, *115*, C12062, doi:10.1029/2010JC006165.

1. Introduction

[2] Icebergs in the Barents Sea present a threat for navigation and offshore installations. The threat could be in a direct form through a collision or via scouring of the ocean floor from grounded icebergs.

[3] The main source of icebergs in the Barents Sea is the Svalbard Archipelago and especially the Austfonna ice cap [*Dowdeswell et al.*, 2008]. The Franz Josef Land glaciers and in particular the Renown Glacier on Wilczek Land [*Kubyshkin et al.*, 2006] are secondary sources. A smaller contribution of icebergs come from glaciers of the northern tip of Novaya Zemlya.

[4] During the last century, icebergs in the Barents Sea have been observed through oceanographic fields campaigns, ice reconnaissance flights and satellite observations. Observational campaigns under the Ice Data Acquisition Program (IDAP [*Spring*, 1994]) from 1988 to 1993 reported that their average and maximum size above the sea surface were 91 m length × 64 m width × 15 m height and 320 m × 279 m × 40 m, respectively. Although a great proportion remain and melt close to the calving area, icebergs were found as far south as 67.2°N in the Barents Sea during the summer of 1929 [*Abramov and Tunik*, 1996]. Further, based on aerial surveys covering the period 1933–1990, *Abramov* [1992] reported the variability of the iceberg distribution within the Barents Sea. The seasonal cycle of the extension of the iceberg distribution, with the southernmost extension occurring in January–May and the northernmost extension during September–October. The interannual variability of the quantity and the geographical distribution of the icebergs depend on their calving rate and the winds. Predominantly northerly and northeasterly winds favor the southern extension of the icebergs. These data have however shown their limitation because they are temporally and spatially sparse.

[5] In order to complete information on icebergs characteristics, *Bigg et al.* [1997] modeled iceberg trajectories over the whole Arctic using a coarse resolution ocean circulation model and sea ice observations from *Bourke and Garrett* [1987].

[6] Here, we propose a more detailed extension of their work applied to the Barents and Kara seas using a high-resolution ice-ocean-iceberg drift model parameterized for the area [*Keghouche et al.*, 2009]. Our main goal is to evaluate the climate-related variability of icebergs in the region. We therefore carried out stochastic simulations of iceberg drift trajectories from July 1985 to December 2005. This allows us to quantify over a period of 20 years, the contribution of climatic factors to the average spatial distribution, the size, the source origin, seasonal and interannual variability of their extension.

[7] The outline of this paper is as follows. Section 2 provides a brief description of the model and the experiment setup. In section 3.1, we focus on the main results by providing an extensive description of the statistics over the period of study. In section 3.2, we describe the modeled seasonal extension of icebergs. In section 3.3, we highlight

[1]Nansen Environmental and Remote Sensing Center, Mohn Sverdrup Center, Bergen, Norway.

0148-0227/10/2010JC006165

mechanisms driving the interannual variability of iceberg drift and in particular the extreme southernmost extension. A summary of the study is given in section 4.

2. Method

2.1. Model

[8] The main characteristics of the iceberg drift model are detailed by *Keghouche et al.* [2009] and summarized in section 2.1.1. For the long-term simulations, we added some model features that we describe in sections 2.1.2 and 2.1.3, concerning the choices for the bottom friction and the melting parameterizations, respectively.

2.1.1. Main Dynamics

[9] The basic equation describing the horizontal motion of an iceberg of mass M is

$$M\frac{d\vec{\mathbf{u}}}{dt} = \vec{\mathbf{F}}_{\mathrm{A}} + \vec{\mathbf{F}}_{\mathrm{W}} + \vec{\mathbf{F}}_{\mathrm{C}} + \vec{\mathbf{F}}_{\mathrm{SS}} + \vec{\mathbf{F}}_{\mathrm{SI}}, \tag{1}$$

where $\vec{\mathbf{u}}$ is the iceberg velocity. The atmospheric force ($\vec{\mathbf{F}}_{\mathrm{A}}\hat{\mathrm{T}}$) and ocean force ($\vec{\mathbf{F}}_{\mathrm{W}}$) act on the cross-sectional area above (below) the water line in a vertical plane (form drag) and a horizontal plane (surface drag) as defined by *Smith and Banke* [1983]. Optimal values for the atmospheric and ocean form drag are 0.70 and 0.25, respectively, based on the best fit for four icebergs observed during 2 months of drift [*Keghouche et al.*, 2009]. In the latter study, the effect of wind waves is included implicitly through the optimization of the atmospheric form drag as with *Smith* [1993]. $\vec{\mathbf{F}}_{\mathrm{C}}$ is the Coriolis force, $\vec{\mathbf{F}}_{\mathrm{SS}}$ is the force due to the sea surface slope and $\vec{\mathbf{F}}_{\mathrm{SI}}$ is the force due to interaction with the sea ice cover. Note that $\vec{\mathbf{F}}_{\mathrm{SI}}$ depends nonlinearly on the sea ice concentration A and the sea ice strength P [*Lichey and Hellmer*, 2001]

$$\mathbf{F}_{\mathrm{SI}} = \begin{cases} 0 & \text{if } A \le 15\%, \\ -\left(\mathbf{F}_{\mathrm{A}}\hat{\mathrm{T}} + \mathbf{F}_{\mathrm{W}} + \mathbf{F}_{\mathrm{C}} + \mathbf{F}_{\mathrm{SS}}\right) + \mathrm{M}\frac{\mathbf{dv}_{\mathrm{si}}}{dt} & \text{if } A \ge 90\% \\ & \text{and } P \ge P_s \\ \frac{1}{2}(\rho_{\mathrm{si}} c_{\mathrm{si}} A_{\mathrm{si}})|\mathbf{v}_{\mathrm{si}} - \mathbf{u}|(\mathbf{v}_{\mathrm{si}} - \mathbf{u}) & \text{otherwise} \end{cases} \tag{2}$$

P_s is set to 13000 N m^{-2}, $\mathbf{v}_{\mathrm{si}}$ is the sea ice velocity, c_{si} is the sea ice coefficient of resistance set to one as by *Lichey and Hellmer* [2001] and A_{si} is the product of the sea ice thickness and the iceberg width. If the sea ice concentration A is lower than 15%, no sea ice force is applied. If A is between 15% and 90%, the sea ice acts as an additional drag force. If A is over 90% and the sea ice strength P surrounding the iceberg is over the threshold value Ps, sea ice and the iceberg form a solid block and the iceberg drifts with the sea ice.

[10] The model inputs are averaged daily to limit memory storage. The atmospheric parameters are from ERA-40 reanalysis of the European Center for Medium-range Weather Forecasting (ECMWF [*Uppala et al.*, 2005]), with 1.125° resolution. The ocean and sea ice variables are supplied by a nested configuration of the Hybrid Coordinate Ocean Model (HYCOM [*Bleck*, 2002]). The inner model covers the Barents and the Kara seas with a horizontal resolution of approximately 5 km and uses 22 vertical hybrid layers. It includes the tides but they are largely filtered out by daily averaging. On seasonal and interannual time scales, we expect the tides to have no influence. The outer model is a version of the TOPAZ3 forecasting system that covers the Atlantic and the Arctic oceans, run without data assimilation [*Bertino and Lisæter*, 2008]. The dynamic part of the sea ice component is based on the elastic-viscous-plastic rheology by *Hunke and Dukowicz* [1997]. The thermodynamic fluxes over open water, ice-covered water, and snow-covered ice are given by *Drange and Simonsen* [1996].

2.1.2. Boundary Conditions and Stability Criterion

[11] When an iceberg hits the bottom, it remains stationary until it has either melted sufficiently to drift off or it is transported toward a deeper region by forces stronger than the frictional force. Based on experimental studies defining friction coefficients of a large ice block on a sand or gravel beach from *Barker and Timco* [2003], we used a static friction coefficient of 0.5 for grounded icebergs. When an iceberg is in a transition mode, moving from a deep region to a region shallower than its immersed part, we used a friction coefficient of 0.35. The icebergs are allowed to roll over, following the *Weeks and Mellor* [1978] stability criterion.

[12] Note that an iceberg is removed if its height is less than 5 meters or if it reaches the nesting zone of the ocean and sea ice model (thick gray lines in Figure 5). The nesting zone represents the last 20 grid cells of the ocean model. We neglect the icebergs that may reenter the domain.

2.1.3. Melting Parameterizations

[13] Among the mechanisms involved in the deterioration of icebergs, we consider only the most important ones: wave erosion, which is the primary source of melting [*White et al.*, 1980; *Bigg et al.*, 1997], lateral melting, and basal melting.

[14] Wave erosion V_{wave} parameterization is taken from *Gladstone and Bigg* [2001], who incorporated a dependency on the sea surface temperature (SST) and the sea ice concentration (m/d)

$$V_{wave} = \left[\frac{1}{6}\left(T_{\mathrm{w}}(1) + 2\right)\right] S_s \left[\frac{1}{2}\left(1 + \cos\left(A^3\pi\right)\right)\right], \tag{3}$$

where $T_{\mathrm{w}}(1)$ is the SST, A is the sea ice concentration, and S_s is the sea state derived from the wind speed. Thus, the wave erosion is damped in presence of sea ice.

[15] Lateral melting $V_{lateral}$ is based on the parameterization of *Kubat et al.* [2007] over the iceberg draft. The empirical estimate of lateral melt rate (m/d) is

$$V_{lateral} = \sum_{k=1}^{n} \left[7.62 \times 10^{-3}(\Delta T(k)) + 1.29 \times 10^{-3}(\Delta T(k))^2\right], \tag{4}$$

where $\Delta T(k)$ is the difference between the sea water temperature and the freezing point temperature at the kth layer interface. The iceberg draft crosses the layers 1 to n of the ocean model.

[16] The estimation of the basal turbulent melting rate V_{basal} (in m/d) follows *Weeks and Campbell* [1973]

$$V_{basal} = 0.58|\mathbf{v}_{\mathrm{w}}(n) - \mathbf{u}|^{0.8} \times \frac{T_{\mathrm{w}}(n) - T(n)}{L^{0.2}}, \tag{5}$$

where $\mathbf{v}_{\mathrm{w}}(n)$ is the water velocity at the iceberg base and $\mathbf{u}$, the iceberg velocity. L is the iceberg length, and $T(n)$ is the iceberg basal temperature. Similar to what it is done for sea ice model basal melting parameterizations, $T(n)$ is the local

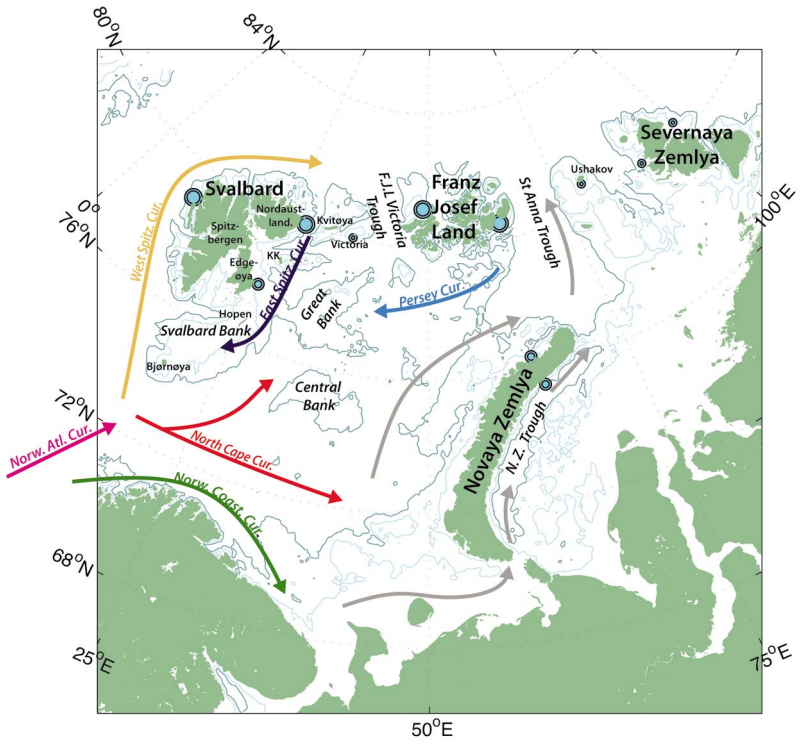

Figure 1. Locations of the different sources of icebergs (solid blue circles) and the main ocean currents. Light and dark blue contour lines are the isobaths at 100 and 200 m, respectively.

freezing point temperature at the iceberg base and $T_w(n)$ is the local water temperature at the iceberg base.

[17] The accuracy of the melting is strongly dependent on the initial estimate of the iceberg size and its location with respect to the sea ice edge and the ocean front. The ocean model temperature and the sea ice concentration compare reasonably well with observations [*Bertino et al.*, 2007]. In the model, the winter ice edge is well defined over the domain but it is overestimated west of Svalbard. During the summer, the model may underestimate the presence of sea ice in the northern region of the Barents Sea while overestimating it in the southern region of the Kara Sea. The ocean temperature error is less than 1°C southwest of the Barents Sea. A data assimilation method is used by I. Keghouche et al. (manuscript in preparation, 2010) to keep the modeled iceberg position close to the observed trajectory of four icebergs drifting in the western part of the Barents Sea from April to July 1990. The melting parameterization provided estimates of the iceberg lifespan which were comparable to the observations.

2.2. Experimental Design

[18] The iceberg discharge is controlled by the glacier speed and the geometric changes in the terminus region [*Van der Veen*, 2002]. These processes occur on smaller scales than we consider in this study. The sources of icebergs in the Barents and Kara seas are marine terminating glaciers and ice cap drainages from Svalbard, Franz Josef Land and Novaya Zemlya. A small amount of icebergs come from the Severnaya Zemlya Archipelago, and Ushakov and Victoria islands. Estimates of iceberg production are given by *Dowdeswell et al.* [2002, 2008], *Hagen et al.* [2003], and *Kubyshkin et al.* [2006]. We define 11 calving sites representing the iceberg production of several outlet glaciers (Figure 1) and adjust the iceberg production rate according to their importance (Table 1). The calving sites are located at a single point near the most active regions, considering the bathymetry and distance to the coastline (≃20 km). (J. A. Dowdeswell and A. Glazovsky (personal communications, 2009) regarding the Svalbard and Russian Arctic regions, respectively, confirmed that this repartition is plausible.)

2.2.1. Size Distribution

[19] During the IDAP program [*Spring*, 1994], extensive observations of icebergs in the Barents Sea from 1988 to 1992 from Aerial Stereo Photography were made. We generate iceberg size characteristics randomly, through a log-normal distribution of the length, width and the freeboard height with mean and variance values, based on the distribution of the observations (Table 2). The width distribution is shown in Figure 2. The freeboard height and the length have similar distribution. Any idealized rectangular tabular iceberg has a depth of four times its freeboard height [*Smith and Banke*, 1983]. Note that these estimates represent the size of icebergs drifting within the Barents Sea and not at their calving site, where they must be larger.

2.2.2. Release Into the Sea

[20] In this study, we chose to release icebergs at a constant calving rate despite indications of increased release from June to September [*Kubyshkin et al.*, 2006]. This allows us to evaluate the seasonal influence of the ocean currents, wind and sea ice on the iceberg characteristics and drift, independently of the seasonal fluctuations in calving rate.

[22] Knowing the annual calving rate and the mean size of icebergs, it is possible to estimate an averaged number of

Table 1. Source Locations of Icebergs and Regional Calving Sites

Area	Total Flux (km^3 yr^{-1}) and Source	Calving Area	Calving Location	Calving Rate (km^3 yr^{-1})
Svalbard	5.5 from *Dowdeswell et al.* [2008] and *Hagen et al.* [2003]	Nordaustlandet and Kvitøya	80°N, 28°E	2.7
	5.5 from *Dowdeswell et al.* [2008] and *Hagen et al.* [2003]	West Spitzbergen	79°N, 10°E	2.2
	5.5 from *Dowdeswell et al.* [2008] and *Hagen et al.* [2003]	Edgeøya	77°N, 25°E	0.6
Franz Josef Land	4.4 from *Kubyshkin et al.* [2006]	Eastern side	80.5°N, 62.8°E	2.64
	4.4 from *Kubyshkin et al.* [2006]	Western side	81.14°N, 48.7°E	1.76
Novaya Zemlya	1.5 from *Kubyshkin et al.* [2006]	Eastern side	75.5°N, 64°E	0.5
	1.5 from *Kubyshkin et al.* [2006]	Western side	76.4°N, 63°E	1.0
Severnaya Zemlya	0.7 from *Kubyshkin et al.* [2006] and *Dowdeswell et al.* [2002]	Eastern side	80.46°N, 99.51°E	0.5
	0.7 from *Kubyshkin et al.* [2006] and *Dowdeswell et al.* [2002]	Western side	80.23°6N, 90.52°E	0.2
Ushakov Island	0.01 from *Kubyshkin et al.* [2006]		80.75°N, 79.42°E	
Victoria Island	0.001 from *Kubyshkin et al.* [2006]		80.03°N, 36.66°E	

icebergs released each day from each source. We consider the release of icebergs as an event occurring at random with a known average rate and independently of the time since the last release. This is expressed by a Poisson process. For each source, the probability to release k icebergs at a given day, knowing the yearly averaged number of release λ is

$$f(k,\lambda) = \frac{\lambda^k e^{-\lambda}}{k!}. \quad (6)$$

[23] The random length of a calved iceberg is picked up from the log normal distribution based on the mean and variance length given in the IDAP database (see section 2.2.1). The width and freeboard height are assigned using the same procedure.

[24] Based on the estimates given in Tables 1 and 2, the annual number of iceberg each year would be $\simeq$19,000–20,000. It is unclear which proportion of these remains grounded near the calving site and which proportion drifts freely in the Barents Sea. To limit the amount of computations, we divided the calving rates from all sites by a factor of 100 and hence launched about 200 icebergs per year. The release occurs from July 1985 to December 2005. Note that no icebergs were released from Victoria Island through the period of study, so this minor source will not be discussed in the following.

3. Results

[25] The simulation starts in July 1985 and ends in December 2005. The average age of icebergs is less than a year and relatively few icebergs persist for more than 2 years (see section 3.1.2). Therefore, we consider the first year and a half as the "spin-up time" for icebergs to spread all over the domain and thus we retain only the last 19 years of simulation. This section presents the results with statistics on different time scales: a 19 year mean for the climatology, monthly means for the seasonal variability and yearly means for the interannual variability.

3.1. Climatology for the Period 1987–2005

3.1.1. Grounded Icebergs

[26] Most of the grounded icebergs are located on shallow waters near their point of calving origin (Figure 3), especially around Nordaustlandet, the two Franz Josef Land sources and the northwest tip of Novaya Zemlya. A small proportion of the grounded icebergs are located along Svalbard bank and the bank starting from the Kara Sea shelf to the edge of Saint Anna Trough. Approximately 77% of the released icebergs become grounded. On average, the icebergs that become grounded spend about 42% of their lifetime motionless. Among the icebergs that are grounded at least once, on average 14% remain grounded for more than 80% of their lifetime. Except for the West Spitzbergen and East Severnaya Zemlya sources, all the others have a large probability (over 80%) of their icebergs becoming grounded at least once. During the IDAP campaign [*Spring*, 1994], the regions north of Hopen and Svalbard bank were identified as regions where icebergs grounded and melted in place. This is observed in the model as well: the proportion of grounded icebergs that spend most of their life grounded is 22% and 32% for iceberg comings from Nordaustlandet and Edgøya, usually traveling southwest.

[27] For some of the calving sites, a significant proportion drift out of the model domain, at a "matured" age, see Table 3. The exceptions are icebergs coming from West Spitzbergen where 45% of the icebergs are lost after 50 days of drift in average.

[28] The friction parameterization had a limited effect on the grounding time. A 1 year simulation with and without the friction parameterization exhibits very little differences in the spatial density map of grounding sites and the average grounding time remained relatively similar (not shown).

3.1.2. Averaged Age

[29] The spatial distribution of the icebergs mean age is heterogeneous (Figure 4). The youngest icebergs are found close to the calving sites, whereas the oldest are often located along the southernmost positions or the northeastern model boundaries, especially southwest of the Barents Sea and along the bank starting from the Kara Sea shelf to the Saint Anna Trough, where icebergs might get grounded (Figure 3). Icebergs are on average 241 days old. About 20% of the icebergs survive more than a year and only 3.3% survive

Table 2. Iceberg Size Characteristics in Meters Based on IDAP Campaign[a]

	Mean	Standard Deviation
Length	91	53
Width	64	37
Freeboard height	15	7

[a] *Spring* [1994].

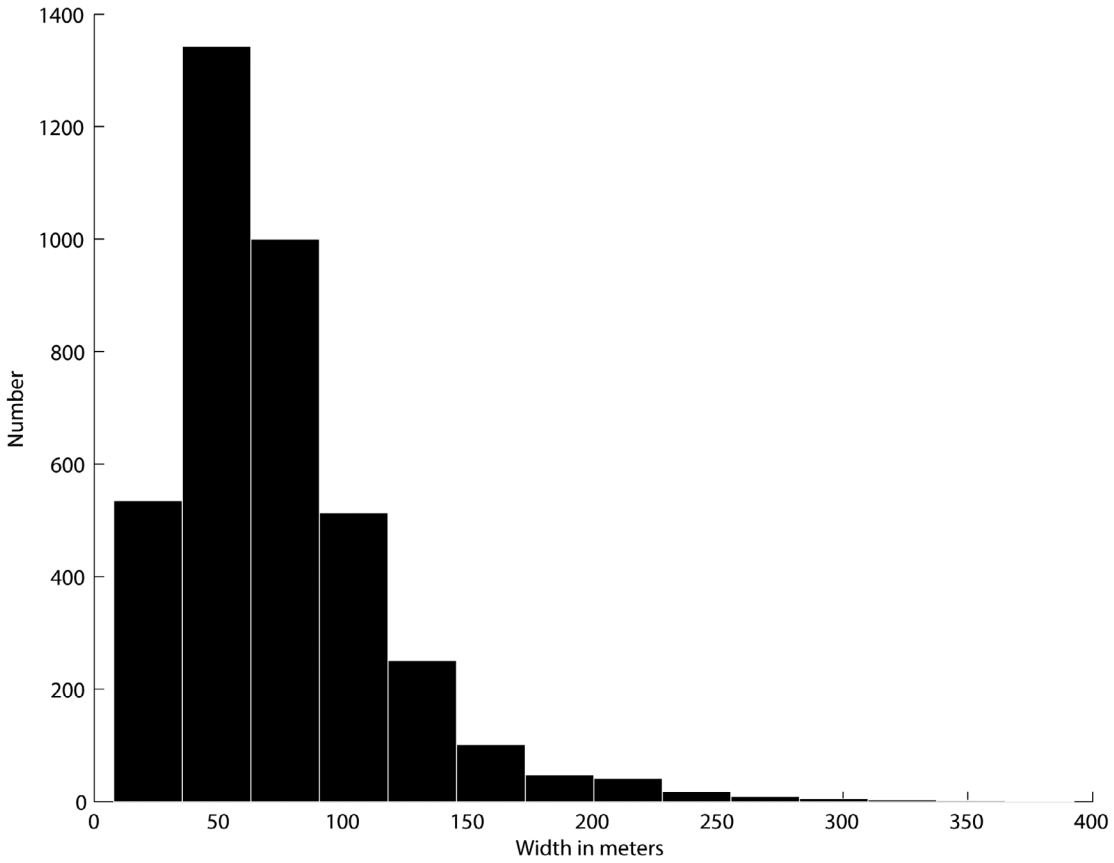

Figure 2. Distribution of iceberg width generated from July 1985 to December 2005.

more than 2 years. The same statistics applied to each calving sources highlights large discrepancies from one source to another (Table 3). The mean age is maximum for icebergs coming from West Severnaya Zemlya (370 days) and East and West Franz Josef Land Archipelago (329 and 314 days, respectively). The oldest iceberg (5.9 years) comes from East Franz Josef Land. The lowest average lifetime of icebergs is 55 days and corresponds to icebergs coming from West Spitzbergen, which leave the model domain relatively quickly, see section 3.1.1.

3.1.3. Annual Probability of Occurrence

[30] A map of the probability of encountering an iceberg within the year shows that most of the icebergs are located close to calving sources and the probability of encountering an iceberg gradually decreases with the distance to the calving site (Figure 5). *Abramov and Tunik* [1996] processed a similar map for the period 1881–1993 based on observations from ships, aerial surveys and ARGOS buoys; 35% of the observations were gathered from 1987 to 1993. The direct qualitative comparison of both maps is challenging, due to the short time overlap and the sparse sampling of the observations. Qualitatively, we observe similar patterns in the iceberg distribution.

3.1.4. Pathways

[31] The spreading of icebergs inside the domain is complex and chaotic, see Figure 8. The total number of icebergs released from each source is reported in Table 3. The implementation allows us to follow the trajectory of icebergs from their calving site. A detailed description of the most important pathways from each source is presented in Figure 6. The modeled drift patterns compare well with the ones described by *Spring* [1994, p. 66], based on Argos buoys placed on 10 icebergs from 1988 to 1992 (not shown). The icebergs that have the largest spread within the domain are coming from East Franz Josef Land and are found in the northern Kara Sea and the northern Barents Sea (Figure 8).

[32] Icebergs coming from the eastern side of Svalbard region stay in the western part of the Barents Sea. They usually move southwest, along the coast, following the East Spitsbergen current over Svalbard bank or even closer to the coast of Svalbard.

[33] Note that icebergs from West Spitsbergen have a relatively small spreading into the domain despite their important number. They have the tendency to quickly drift off the model boundary, see section 3.1.1. The icebergs drifting in the central Kara Sea originate mainly from East Novaya Zemlya.

3.2. Seasonal Variability

[34] The difference between the mean iceberg density during the summer months and the mean iceberg density during the winter months from 1987 to 2005 is an indicator of the seasonal variability, see Figure 7. Here, the summer is defined from 15 May to 15 November and the winter consists of the other months of the year.

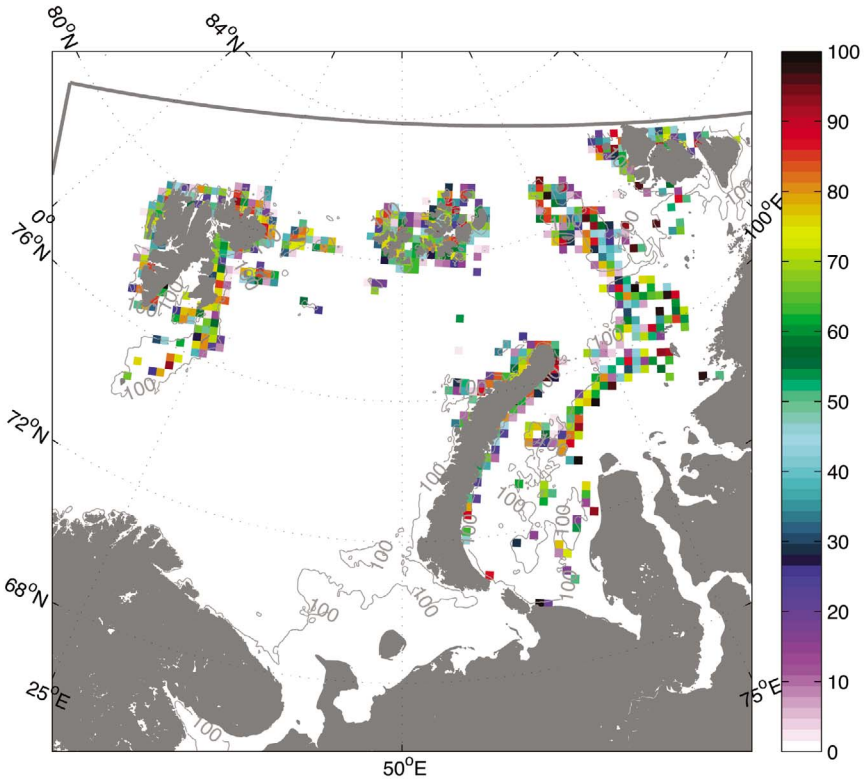

Figure 3. Probability (%) of having an iceberg grounded within a 25 × 25 km grid cell during the period 1987–2005. Gray contours are isobaths at 100 m. The northern boundary of the model is shown by the thick gray line.

[35] In general, the number of icebergs close to the calving sources is higher in winter than in summer. The extreme southernmost positions occur during the summer period, in accordance with *Abramov* [1992]. The presence of strong and highly concentrated sea ice in winter slows down the motion of iceberg and limit their extension. Maximum iceberg extension occurs in June–July and the minimum iceberg extension occurs in October–November most of the years.

[36] In Figure 7 (left), we also find a seasonal imbalance in the iceberg density on each sides of the islands producing icebergs (e.g., Franz Josef Land, Novaya Zemlya and Svalbard). There are more icebergs located on the east (west) of the island in winter (summer). This might be due to the preponderance of northeasterlies in winter, which transport the icebergs away if the source is on the west and maintain them close to their source if the latter is on the east of the island.

[37] We observe a seasonal variability of the iceberg extension, though we did not consider the seasonality of the calving. It suggests that seasonal variability of forcing fields, i.e., the wind fields, ocean currents and sea ice are important for the seasonal spreading of icebergs. Finally, we looked at the distribution of iceberg released in summer and compared it with the distribution of iceberg released in winter (Figure 7

Table 3. For Each Iceberg Source, Estimates of the Mean Iceberg Age, the Percentage of Icebergs Leaving the Model Domain, Their Mean Age at That Time and the Total Number of Icebergs Based on Simulations From 1987 to 2005[a]

Source Number	Source Name	Mean Age (days)	Percentage Leaving the Model Boundary	Mean Age When Leaving the Model Boundary (days)	Maximum Age (days)	Number And Proportion
1	Nordaustlandet	260	16.2	250	1966	800 (22.2%)
2	West Spitzbergen	55	46.7	53	294	666 (18.5%)
3	Edgeøya	156	4.1	106	526	176 (4.9%)
4	West Franz Josef Land	314	34.2	214	1288	529 (14.7%)
5	East Franz Josef Land	329	14.8	325	2146	775 (21.6%)
6	East Novaya Zemlya	249	2.4	521	911	168 (4.7%)
7	West Novaya Zemlya	268	5.4	528	1284	276 (7.7%)
8	East Severnaya Zemlya	122	100.0	115	1476	149 (4.1%)
9	West Severnaya Zemlya	370	71.7	354	1407	53 (1.5%)
10	Ushakov Island	283	33.3	338	338	3 (0.1%)

[a]See Figure 1 for the location of the sources.

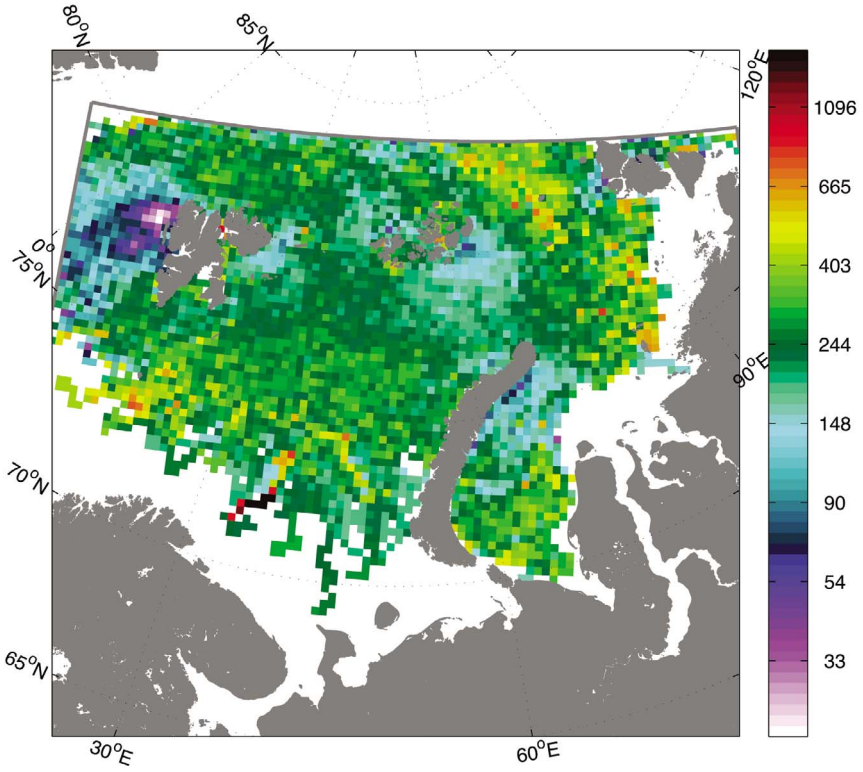

Figure 4. Average age (days) during the period 1987–2005 with a grid cell resolution of 25 × 25 km. The scale is logarithmic. The northern boundary of the model is shown by the thick gray line.

(right)). The icebergs released in summer have the largest spreading. Therefore, we suspect that introducing seasonal variability in the calving would intensify the seasonal variability of the iceberg spreading.

3.3. Interannual Variability of the Iceberg Extension Over the Domain

[38] In this section we focus on the mechanisms driving the spatial extension of the icebergs, by retaining them not far from the calving sites some years or transporting them very far south some others. In addition we analyze the extreme southernmost extension in our model.

3.3.1. Iceberg Extension

[39] The interannual variability of iceberg spreading is large. The year with the smallest spreading in the domain and the year with the largest one are shown in Figure 8. In order to evaluate the interannual variability of the iceberg spreading, we define a measure for the iceberg extension. The iceberg extension is the sum of any grid cell area where an iceberg has drifted independently of the number of passages within that grid cell. The annual time series have a strong variability and highlight a weak decreasing trend (Figure 9) over the period of study. Years with the largest spreading are 1988, 1987, 2003, and 1992 (sorted from the largest to the smallest), whereas years with the smallest extensions are 2000, 1997, 2001, and 1995 (from the smallest to the largest). If we remove the trend from the time series (not shown), the extrema appear in the second half of 1987–2005 period with a minimum kept in 2000 and a maximum in 2003. The variability of the iceberg extent has a time scale longer than 2 years (autocorrelation of 0.5, with 1 year lag), indicating a potential for prediction of this parameter.

[40] In order to gain some insight on the mechanisms involved in the interannual variability of the iceberg spread in the domain, we study the relationship between the iceberg extent and the main forcing components of our model, i.e., the atmosphere, ocean currents and sea ice. Results from correlation analysis are summed up in Table 4. It reveals two mechanisms acting on the iceberg extent: one dynamic and the other thermodynamic.

3.3.1.1. Dynamics

[41] We found large differences in the correlation between different sea ice quantities and the iceberg extent. The annual sea ice area within the domain has a correlation of 0.64 with the iceberg extent, whereas the annual sea ice volume has no significant correlation. It implies that the iceberg extent is independent of the ice thickness within the domain. Note that our iceberg drift model is constraint nonlinearly by the surrounding sea ice concentration and thickness, as described in equation (2). It is important to understand whether the high correlation between the sea ice area and iceberg extent is due to a grasping effect of sea ice on the icebergs or rather a common reaction to an external force. The mean annual percentage that the icebergs drift with the sea ice varies between 15% and 30%. The time series are correlated at $\simeq$0.37 with the iceberg extent and $\simeq$0.63 with iceberg extent from the preceding year. Therefore, the intermittent movement of icebergs driven by sea ice is not the main mechanism controlling the iceberg extent. Concerning the sea ice volume transport into the domain, it is correlated at $\simeq$0.41 with the iceberg extent and at $\simeq$0.46 with the sea ice area. The

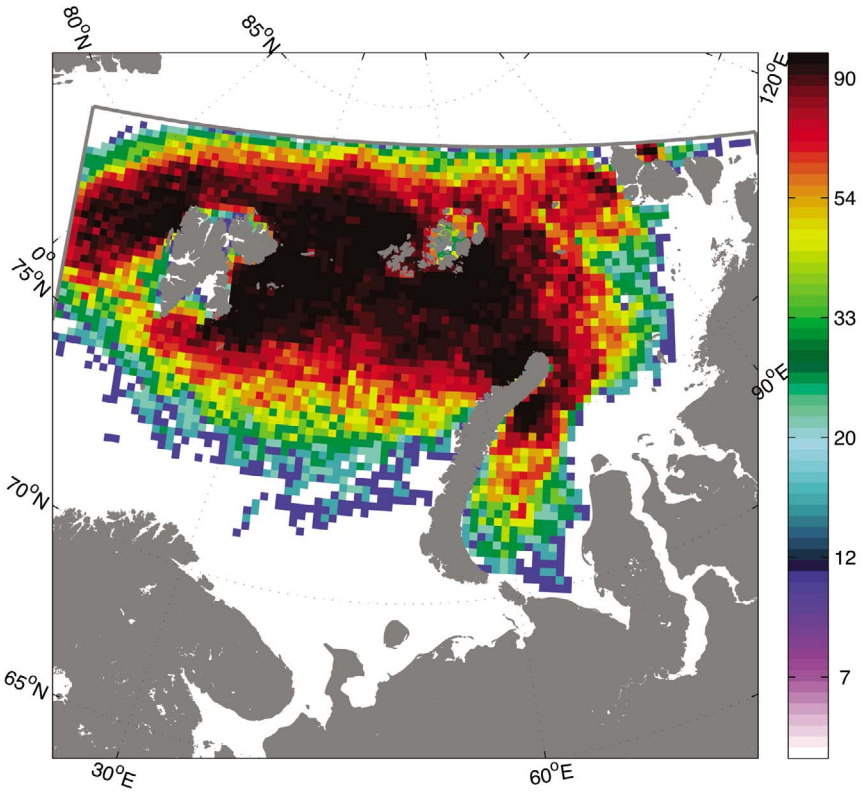

Figure 5. Probability (%) of encountering an iceberg within a year in the domain from 1987 to 2005 within a 25 × 25 km grid cell. The scale is logarithmic. The northern boundary of the model is shown by the thick gray line.

correlation between the sea ice volume transport into the domain, the sea ice area and the iceberg extent suggests a relationship with the atmospheric forcing, which is analyzed in more detail below.

[42] Regression analysis of the winter mean sea level pressure (MSLP) anomalies over the North Atlantic and the Arctic with the winter sea ice extent over the Barents Sea during the period 1967–2002 [*Sorteberg and Kvingedal*, 2006], reveals that higher than normal MSLP over Svalbard region favors large sea ice extent. It leads to a weakening of the westerlies and more locally in the Barents region, to anomalous southward geostrophic winds over the period 1967–2002. We found similar results (not shown) by applying the regression analysis on the iceberg extent during our period of study 1987–2005. We therefore suggest that the northerly winds are the principal actors enhancing iceberg extent.

3.3.1.2. Thermodynamics

[43] The SST over the domain is anticorrelated with the iceberg extent with a value of −0.49. Interannual variability of the mean SST anomaly is anticorrelated at $\simeq -0.66$ to the annual mean age anomaly of icebergs during the year of their calving. It indicates the importance of the thermodynamics in the age and therefore the extension of icebergs.

[44] The warm Atlantic Water (AW) enters the Barents Sea between Norway and Svalbard. When passing through the Barents Sea, the AW is strongly modified by cooling, mixing and freezing during winter before entering the Arctic Ocean [*Ingvaldsen et al.*, 2004a]. The modeled positive transport into the Barents Sea has a negative correlation of −0.28 with the iceberg extent over the 19 years of simulation. It increases to −0.66 with a lag of 1 year. This 1 year lag is similar the time needed for the heat anomalies to spread within the Barents Sea. The variability of the inflow to the Barents Sea is highly dependent on the winds [*Ingvaldsen et al.*, 2004b]. We processed a linear regression and correlation analysis of the MSLP anomalies with the iceberg extent lagged by 1 year (Figure 10). This indicates that the iceberg extent is correlated at $\simeq 0.6$ with MSLP anomalies over the Svalbard region. Positive MSLP anomalies over Svalbard-Nordic seas region may limit the intensity of the Atlantic inflow to the Barents Sea due to a reduced cyclonic activity over the Nordic Seas or enhanced northerly winds. It limits the heat content of the Barents Sea the following year, increases the mean age of icebergs and thus their potential extension. Note that we did not find any connection between the iceberg extent and large-scale atmospheric patterns such as the North Atlantic Oscillation or Arctic Oscillation with either a zero or a 1 year time lag.

3.3.2. Extreme Southernmost Extension

[45] In order to analyze the geographical locations of the southernmost icebergs, we first analyze the latitudinal distribution of the icebergs occurrence within different latitudinal ranges at yearly time scale (Figure 11). The iceberg position is stored once per day, thus an occurrence is a daily event. Any occurrence south of 75°N is considered to be "extreme". Considering the number of occurrences rather than the number of individuals allows us, to weight the

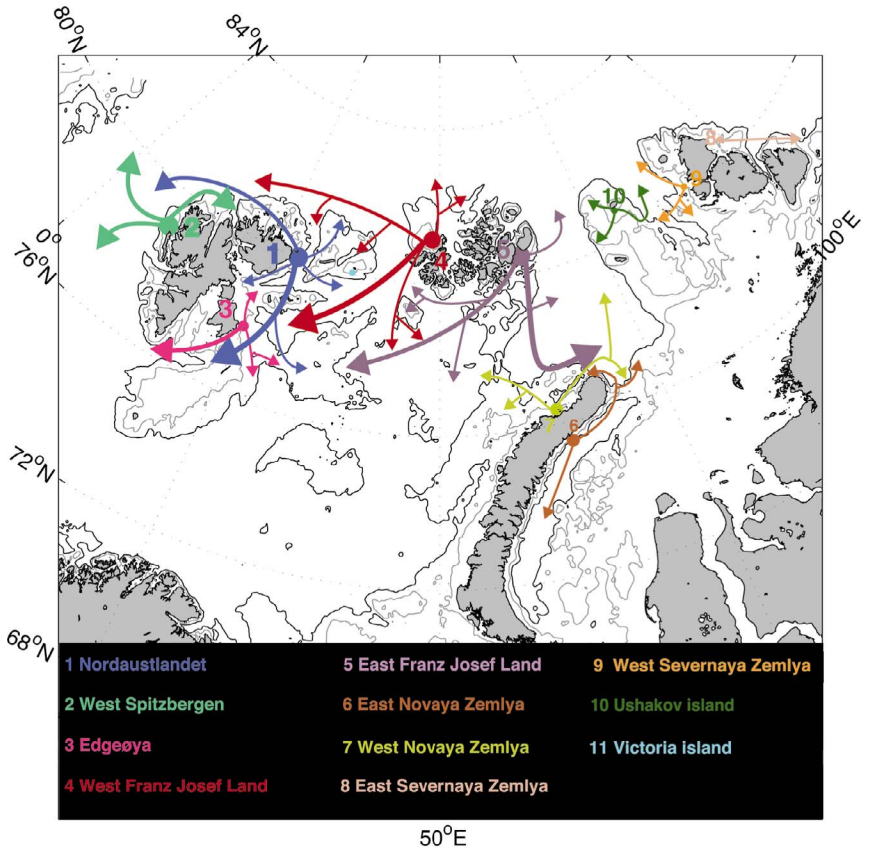

Figure 6. Pathways of icebergs from their calving site based on the model runs covering the period 1985–2005. Main pathways are shown with larger arrows.

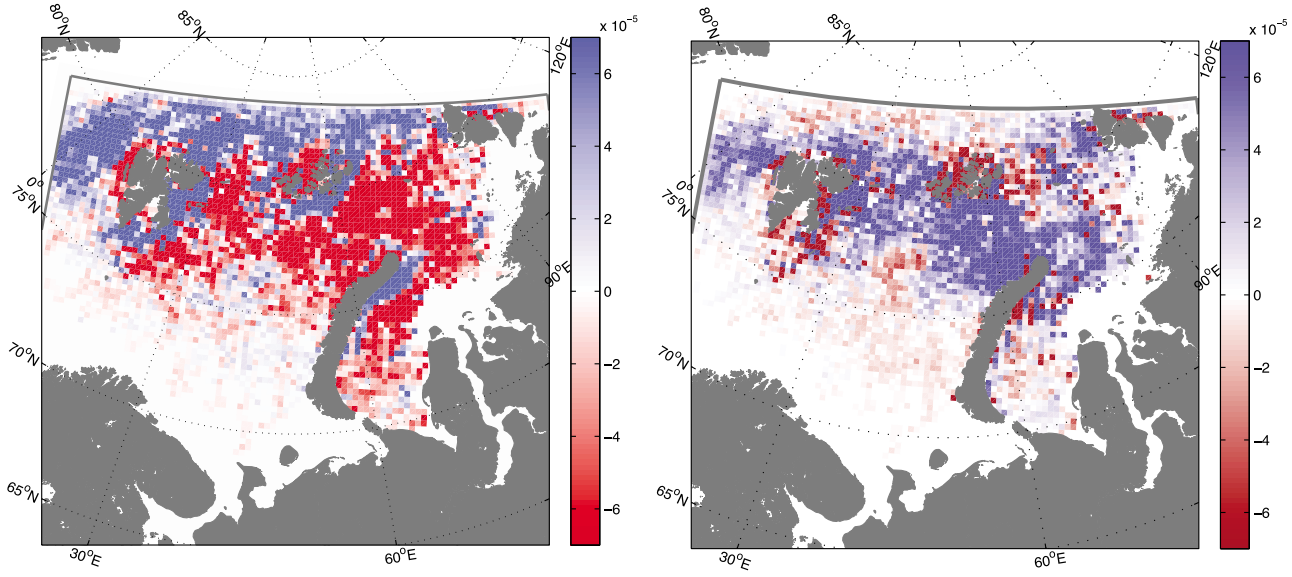

Figure 7. (left) Mean winter iceberg density minus the mean summer iceberg density from 1987 to 2005 with a grid cell resolution of 25 × 25 km. The northern boundary of the model is shown by the thick gray line. (right) Density of icebergs released in winter minus density of icebergs released in summer from the same period and same grid as Figure 7 (left).

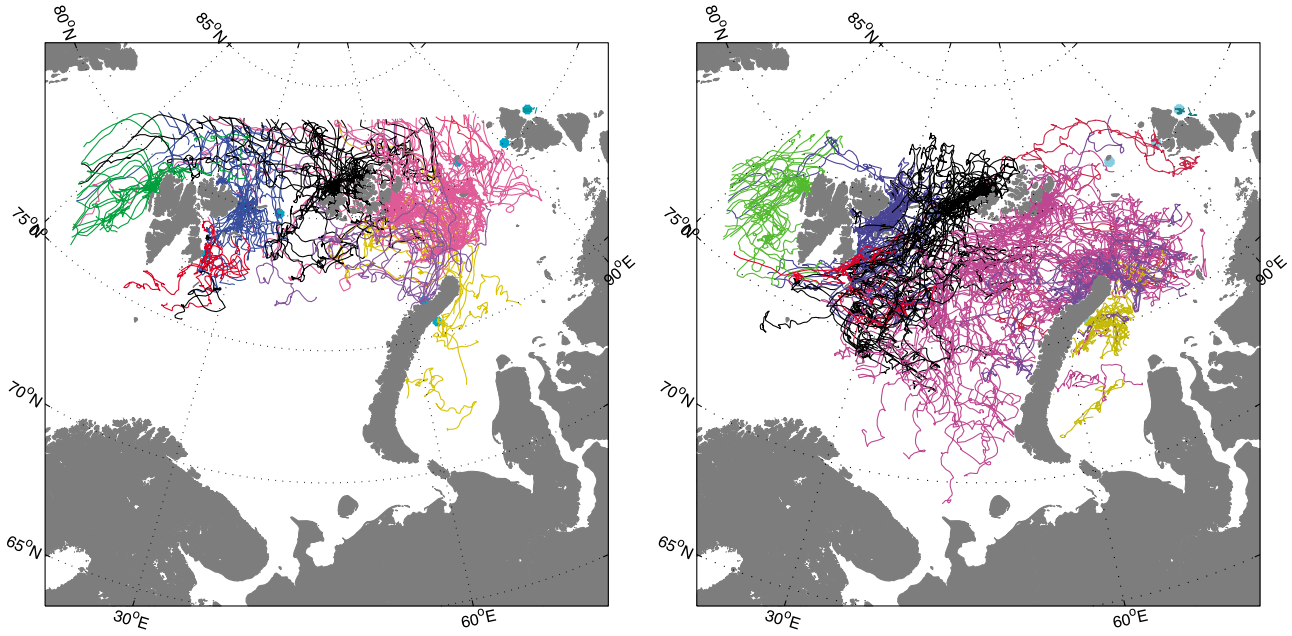

Figure 8. Iceberg trajectories from (left) the year 2000 and (right) the year 2003. The colors depend on the source origin.

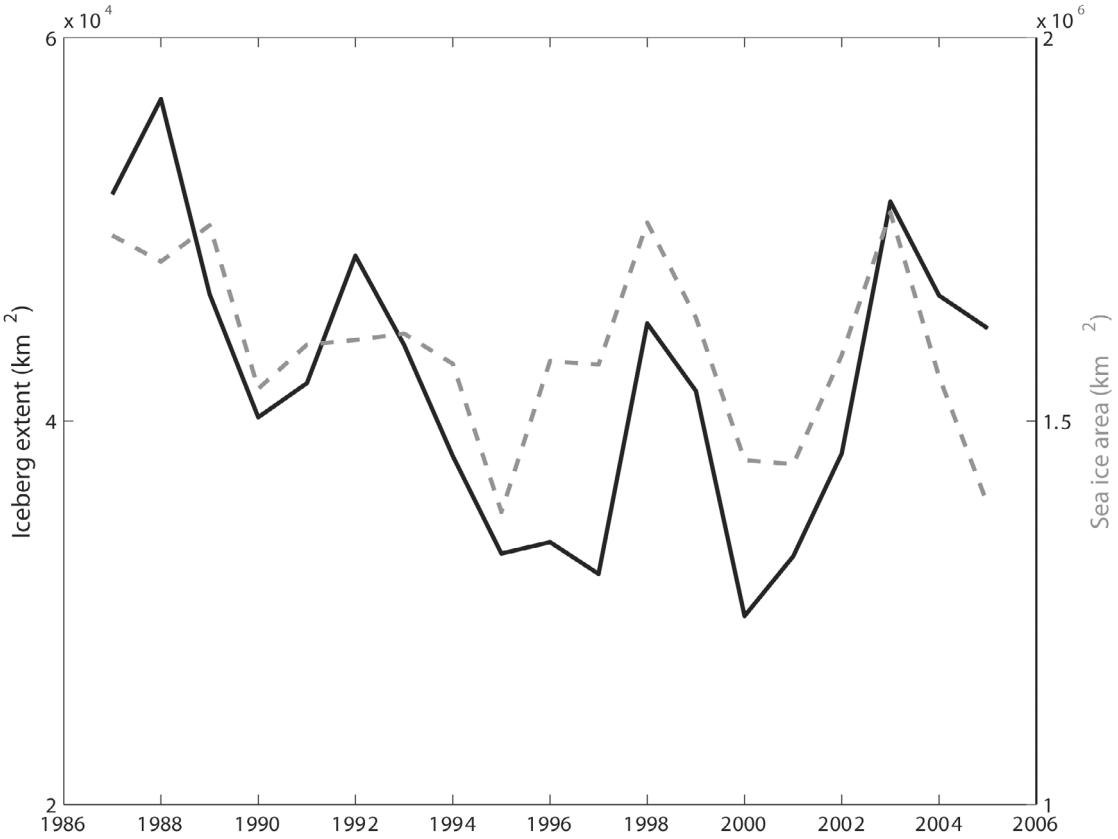

Figure 9. Annual mean of the iceberg extent (solid black) and ice area (dotted gray) over the model domain.

Table 4. Correlations Between the Annual Iceberg Extension and the Annual Sea Ice Area, the Sea Ice Volume, Sea Ice Transport Into the Domain, the Positive Transport Along Norway-Svalbard Section, the Sea Surface Temperature, for the Period 1987–2005

	Sea Ice Area	Sea Ice Volume	Sea Ice Transport[a]	Positive Transport Along Norway-Svalbard Section	Sea Surface Temperature
			No Time Lag		
With trend	0.68[b]	0.13[b]	0.44[c]	−0.30[d]	−0.51[b]
Without trend	0.64[b]	0.03[b]	0.41[c]	−0.28[d]	−0.49[b]
			A 1 Year Time Lag		
With trend				−0.65[b]	
Without trend				−0.66[b]	

[a]From Svalbard to Severnaya Zemlya
[b]Here $p \leq 0.1$ with a t test that takes into account the autocorrelation of the iceberg extent and $p \leq 0.05$ with a t test neglecting the autocorrelation of the iceberg extent.
[c]Here $p \leq 0.2$ with a t test that takes into account the autocorrelation of the iceberg extent and $p \leq 0.1$ with a t test neglecting the autocorrelation of the iceberg extent.
[d]The correlation is not significant.

icebergs with respect to the time spent south. We observe that the years 2003, 1993, 2002, and 1999 have the largest number of occurrences south of 75°N over the domain. To complete the information about the the spatial spread, we introduce another quantity: the meridional percentage of iceberg occurrence found south of 75°N (see Figure 12). The latter quantity exhibits discrepancies on a regional scale. Extreme southernmost extensions occurred at different times in the Barents and Kara seas. For example, the 2003 and 1993 southernmost extension is large for both regions, while the large spread during the years 2002 and 1999 was only in the Kara Sea.

[46] Most of the icebergs passing 75°N are located in the western part of the Kara Sea with a peak between 60°E and 65°E, except in 2002 when the peak shifted to 65°E–70°E. Southernmost Kara Sea icebergs come primarily from East Novaya Zemlya glaciers, and from West Novaya Zemlya and East Franz Josef Land for some years.

[47] In the Barents Sea, the icebergs passing 75°N are concentrated in the eastern part, except in 1993 when a large amount of icebergs passed between 20°E and 30°E as well. The year with the largest southernmost extension is 2003, with icebergs mostly concentrated between 35°E and 55°E. Southeast Barents Sea icebergs come mainly from Franz Josef Land glaciers and West Novaya Zemlya. The same year (2003), icebergs from West Severnaya Zemlya were also found in the south of the Barents Sea (Figure 13). Southwest Barents Sea icebergs come mainly from West Franz Josef Land glaciers and possibly Edgeøya or Nordaustlandet. In relation to the dynamic and thermal mechanisms suggested previously, a positive MSLP anomaly was present over the Svalbard region for all of the years during which the iceberg extent in the Barents Sea was at its southernmost extreme (2003, 1993, 1988, and 1996). During these periods the transport of AW into the Barents Sea was also lower than the average value with the exception of the year 1996. In 1996 fewer icebergs drifted south of the Barents Sea compared to the other years, yet their lifespan allowed for them to drift past 75°N impacting the number of occurrences. The year 1996 is

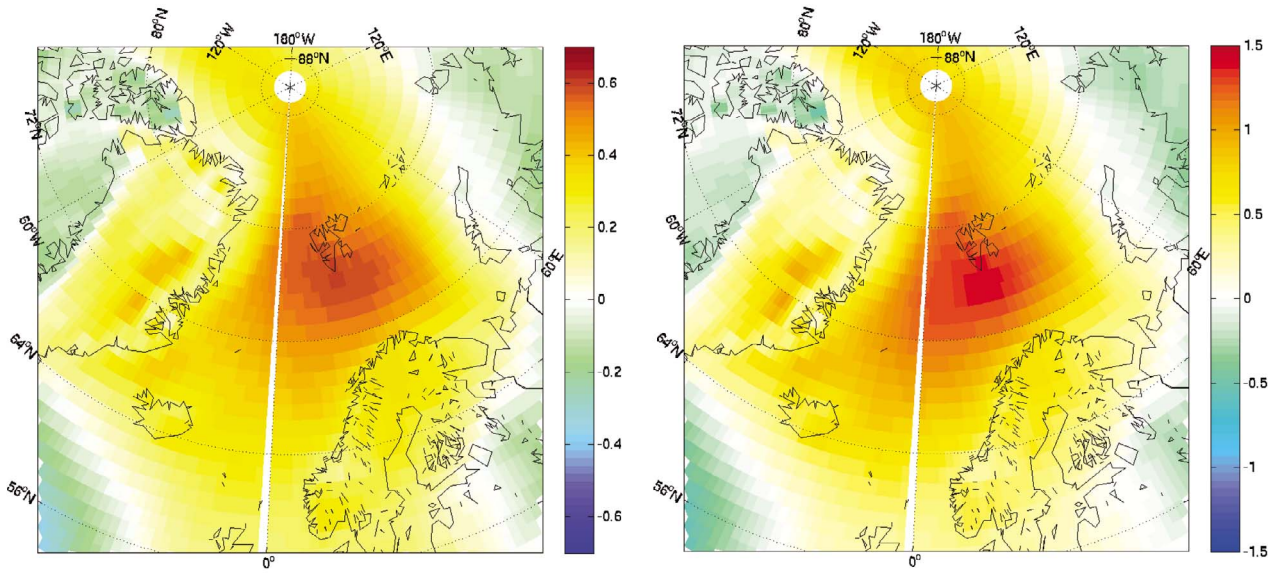

Figure 10. Linear (left) correlation and (right) regression between the annual MSLP anomalies and the annual mean iceberg extent lagged by 1 year for the period 1987–2005.

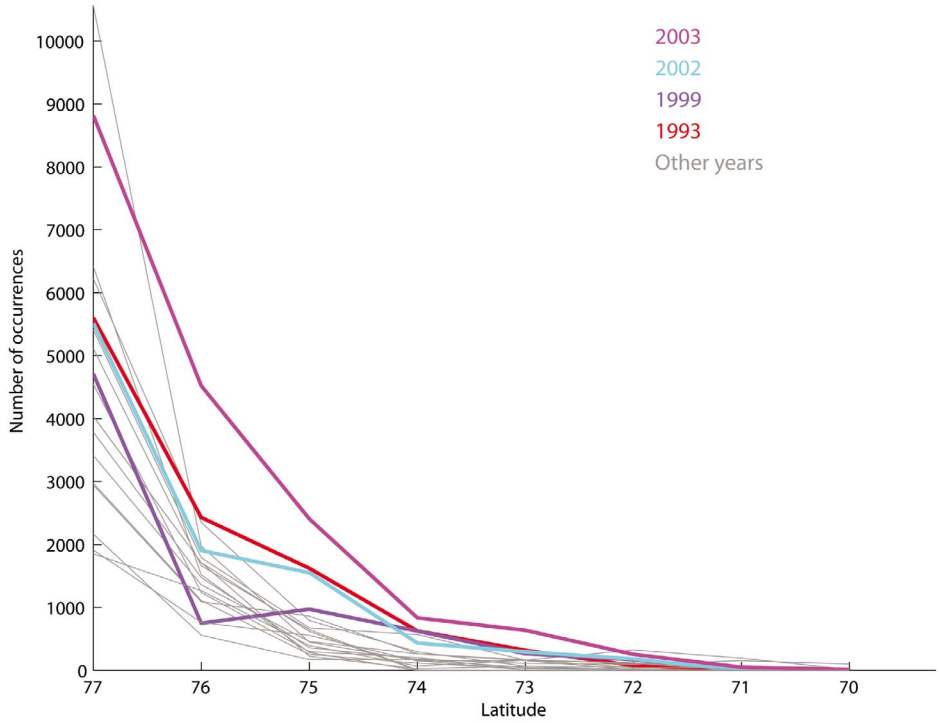

Figure 11. Annual occurrence of icebergs at various latitudes south of 77°N for the period 1987–2005. The colored lines correspond to the years with the largest number of iceberg occurrence south of 75°N within the model domain.

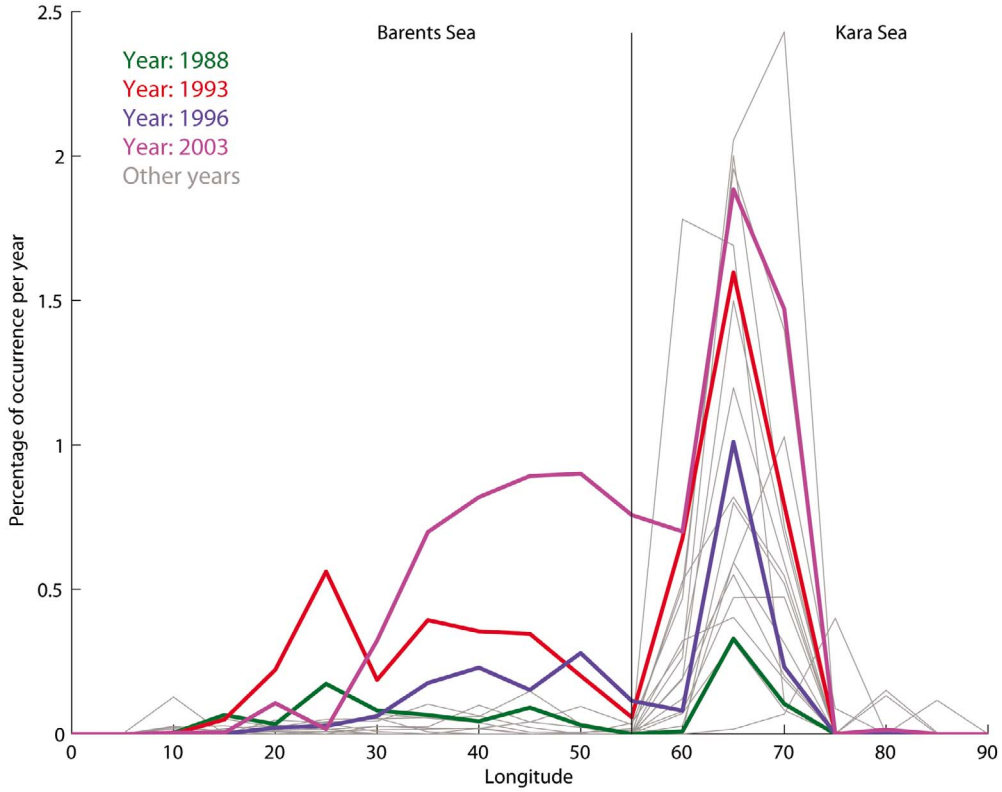

Figure 12. Annual percentage of occurrence found south of 75°N depending on their longitude location for the period 1987–2005. The number was split by classes of 5° of longitude. The colored lines correspond to the years with the largest number of occurrences south of 75°N within the Barents Sea area.

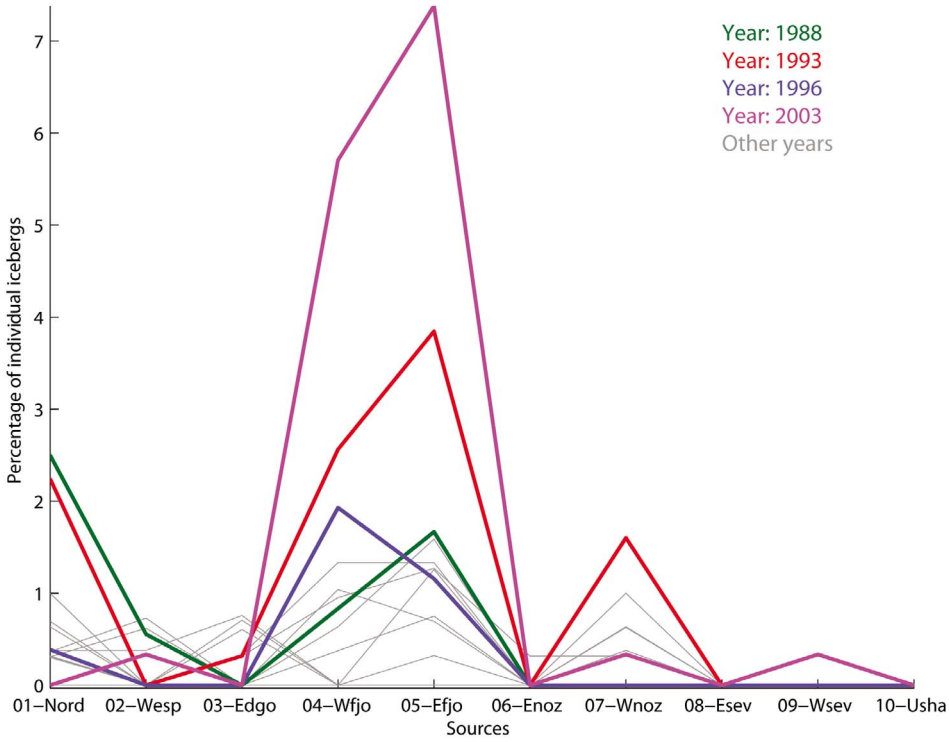

Figure 13. Annual percentage of icebergs from each source found south of 75°N for the period 1987–2005. The colored lines correspond to the years with the largest number of occurrences south of 75°N within the Barents Sea area.

extreme in the sense that the anomalous southeasterly winds were observed.

[48] Note that the northernmost extension occurred in 1989 for the Kara Sea, while for the Barents Sea, 1999, 2000, and 2005 are years with the northernmost extension. Note that for the southernmost extension the year 2003 is extreme in terms of the proportion of icebergs that drift southeast of the Barents Sea. A field campaign in May of that year observed a surprisingly large number of icebergs in that region [*Zubakin et al.*, 2004]. In our simulation, a group of icebergs is observed at the same location at the same time. This group came from East Franz Josef Land and most of the icebergs were calved during the same period, from late September 2002 until late October 2002. Despite of their large spread, they followed similar drift patterns. A persistent southward drift was followed by a northward (wind), transporting them northward. Each northward drift lasting approximately 20 days.

4. Conclusion

[49] This study is an attempt to describe the iceberg distribution in the Barents and Kara seas from a modeling perspective. Lack of iceberg drift observations in the eastern part of the domain makes a thorough validation complicated. Using iceberg drift observations in the western region of the Barents Sea in 1990, *Keghouche et al.* [2009] obtained modeled trajectories, which were reasonably consistent and I. Keghouche et al. (manuscript in preparation, 2010) show that the melting parameterization is in accordance with the observed iceberg lifespan when icebergs are replaced close to the observed positions and when the initial mass is accurately estimated. The average age and extent of icebergs are somewhat uncertain but the qualitative mechanisms explained in this study should remain valid.

[50] Simulations of iceberg trajectories were performed from July 1985 to December 2005. The first 1.5 years of the simulation are not used to allow sufficient time for the model to spin up. Maps of iceberg density, potential locations subject to grounding complement existing statistics of icebergs characteristics in the Barents Sea derived from sparse oceanographic and aerial field campaigns [*Abramov and Tunik*, 1996; *Spring*, 1994]. The model suggests that the icebergs follow preferential pathways (Figure 6) from their respective calving sources. We found that icebergs originating from East Franz Josef Land have the largest spread over the domain.

[51] Simulations confirm the seasonal cycle of the southernmost extension observed by *Abramov* [1992]. We observe a large seasonal variability of the iceberg extension, though we did not consider the seasonality of the calving. It suggests that seasonal variability of forcing fields, i.e., the wind fields, ocean currents and sea ice are very important for the seasonal spreading of iceberg.

[52] We observed large interannual variability of the iceberg extent with a weak decreasing trend, in accordance with the observed sea ice extent. The latter two quantities are also strongly correlated when they are detrended (0.64). *Sorteberg and Kvingedal* [2006] found that MSLP higher than normal over Svalbard region enhance sea ice extent in the Barents Sea through enhanced northerly winds. Following their approach, regression and linear correlation analysis

of the iceberg extent over our period of study leads to a similar conclusion for the iceberg extent.

[53] We also suggest that the positive transport into the Barents Sea is a potential predictor of iceberg extent, as they have a 1 year lag correlation of −0.66. The AW affects the heat balance in the Barents Sea and therefore the iceberg lifetime. The inflow into the Barents Sea is highly dependent on the winds [*Ingvaldsen et al.*, 2004b]. A linear regression and correlation analysis of the MSLP anomalies with the iceberg extent lagged by 1 year shows that MSLP higher than normal east of the Greenland Sea and south of Svalbard region enhanced iceberg extent the following year. We suggest that this is due to the fact that a reduced cyclonic activity over the Nordic Seas limits the intensity of the warm inflow into the Barents Sea and reduces the heat content of the Barents Sea the next year, increasing the mean age of iceberg and thus their potential extension. Finally, the model was able to simulate the observed extreme extension of icebergs originating from Franz Josef Land in May 2003.

[54] **Acknowledgments.** The authors acknowledge Trond Mohn care of Frank Mohn AS for an endowment to the Mohn-Sverdrup Center. This work has also received partial funding from the MERSEA Integrated Project from the European Commission 6th Framework Program and a grant for computer time from the Norwegian Program for Supercomputing (NOTUR). We thank Annette Samuelsen and Knut A. Lisæter for useful comments on the manuscript. We are also grateful to Asgeir Sorteberg for valuable discussions on some of the results and to anonymous reviewers for their constructive comments.

References

Abramov, V. A. (1992), Russian iceberg observations in the Barents Sea, 1933–1990, *Polar Res.*, *11*, 93–97.

Abramov, V. A., and A. Tunik (1996), *Atlas of Arctic Icebergs: The Greenland, Barents, Kara, Laptev, East-Siberian, and Chukchi Seas, and the Arctic Basin*, Backbone, Paramus, N. J.

Barker, A., and G. Timco (2003), The friction coefficient of a large ice block on a sand/gravel beach, paper presented at 12th Workshop on the Hydraulics of Ice Covered Rivers, Comm. on River Ice Processes and the Environ., Edmonton, Alberta, Canada.

Bertino, L., and K. A. Lisæter (2008), The TOPAZ monitoring and prediction system for the Atlantic and Arctic oceans, *J. Oper. Oceanogr.*, *1*, 15–18.

Bertino, L., I. Keghouche, and K. A. Lisæter (2007), KARBIAC JIP phase 2, hindcast of the Barents Sea April 1987–May 1988, *Tech. Rep. 282*, Nansen Environ. and Remote Sens. Cent., Bergen, Norway.

Bigg, G. R., M. R. Wadley, D. P. Stevens, and J. A. Johnson (1997), Modelling the dynamics and thermodynamics of icebergs, *Cold Reg. Sci. Technol.*, *26*, 113–135.

Bleck, R. (2002), An oceanic general circulation model framed in hybrid isopycnic-cartesian coordinates, *Ocean Modell.*, *4*, 55–88.

Bourke, R., and R. Garrett (1987), Sea ice thickness distribution in the Arctic Ocean, *Cold Reg. Sci. Technol*, *13*, 259–280.

Dowdeswell, J. A., et al. (2002), Form and flow of the Academy of Sciences Ice Cap, Severnaya Zemlya, Russian High Arctic, *J. Geophys. Res.*, *107*(B4), 2076, doi:10.1029/2000JB000129.

Dowdeswell, J. A., T. Benham, T. Strozzi, and J. Hagen (2008), Iceberg calving flux and mass balance of the Austfonna ice cap on Nordaustlandet, Svalbard, *J. Geophys. Res.*, *113*, F03022, doi:10.1029/2007JF000905.

Drange, H., and K. Simonsen (1996), Formulation of air-sea fluxes in ESOP2 version of MICOM, *Tech. Rep. 125*, Nansen Environ. and Remote Sens. Cent., Bergen, Germany.

Gladstone, R. M., and G. R. Bigg (2001), Iceberg trajectory modeling and meltwater injection in the Southern Ocean, *J. Geophys. Res.*, *106*, 19,903–19,915.

Hagen, J., J. Kohler, K. Melvold, and J. Winther (2003), Glaciers in Svalbard: Mass balance, runoff and freshwater flux, *Polar Res.*, *22*, 145–159.

Hunke, E., and J. Dukowicz (1997), An elastic-viscous-plastic model for sea ice dynamics, *J. Phys. Oceanogr.*, *27*, 1849–1867.

Ingvaldsen, R., L. Asplin, and H. Loeng (2004a), The seasonal cycle in the Atlantic transport to the Barents Sea during the years 1997–2001, *Cont. Shelf Res.*, *24*, 1015–1032.

Ingvaldsen, R., L. Asplin, and H. Loeng (2004b), Velocity field of the western entrance to the Barents Sea, *J. Geophys. Res.*, *109*, C03021, doi:10.1029/2003JC001811.

Keghouche, I., L. Bertino, and K. Lisæter (2009), Parameterization of an iceberg drift model in the Barents Sea, *J. Atmos. Oceanic Technol.*, *26*, 2216–2227.

Kubat, I., M. Sayed, S. Savage, T. Carrieres, and G. Crocker (2007), An operational iceberg deterioration model, paper presented at Seventeenth (2007) International Offshore (Ocean) and and Polar Engineering Conference, Int. Soc. of Offshore and Polar Eng., Lisbon.

Kubyshkin, N., I. Buzin, A. Glazovsky, and A. Skutin (2006), Determination of the area of generation of big icebergs in the Barents Sea—Temperature distribution analysis, paper presented at Sixteenth (2006) International Offshore (Ocean) and Polar Engineering Conference Proceedings, Int. Soc. of Offshore and Polar Eng., San Fancisco, Calif.

Lichey, C., and H. H. Hellmer (2001), Modeling giant-iceberg drift under the influence of sea ice in the Weddell Sea, Antartica, *J. Glaciology.*, *47*, 452–460.

Smith, S. D. (1993), Hindcasting iceberg drift using current profiles and winds, *Cold Reg. Sci. Technol.*, *22*, 33–45.

Smith, S. D., and E. G. Banke (1983), The influence of the winds, currents and towing forces on the drift of icebergs, *Cold Reg. Sci. Technol.*, *6*, 241–255.

Sorteberg, A., and B. Kvingedal (2006), Atmospheric forcing on the Barents Sea winter ice extent, *J. Clim.*, *19*, 4772–4784.

Spring, W. (1994), Ice data acquisition program, summary report, *Tech. Rep. 472-37*, Mobil Res. and Dev. Corp., Dallas E&P Eng., Dallas, Texas.

Uppala, S. M., et al. (2005), The ERA-40 re-analysis, *Q. J. R. Meteorol. Soc.*, *131*, 2961–3012.

Van der Veen, C. (2002), Calving glaciers, *Prog. Phys. Geogr.*, *26*, 96–122.

Weeks, W., and W. Campbell (1973), Icebergs as a fresh water source: An appraisal, *J. Glaciol.*, *12*, 207–233.

Weeks, W., and M. Mellor (1978), Some elements of iceberg technology, technical report, U. S. Army Cold Reg. Res. and Eng. Lab., Hanover, N. H.

White, F. M., M. L. Spaulding, and L. Gominho (1980), Theorical estimates of various mechanisms involved in iceberg deterioration in open ocean environment, *Tech. Rep. CG-D-62-80*, U.S. Coast Guard, Washington, D. C.

Zubakin, G. K., A. K. Naumov, and I. V. Buzin (2004), Estimations of the ice and iceberg distribution in the Barents Sea, paper presented at Fourteenth (2004) International Offshore (Ocean) and Polar Engineering Conference, Int. Soc. of Offshore and Polar Eng., Toulon, France

L. Bertino, F. Counillon, and I. Keghouche, Nansen Environmental and Remote Sensing Center, Mohn Sverdrup Center, Thormøhlensgt. 47, N-5006 Bergen, Norway. (intissar.keghouche@nersc.no)